6-1-2022

Monofacial Vs Bifacial Solar Photovoltaic Systems In Snowy Environments

Koami Soulemane Hayibo
Western University, khayibo@uwo.ca

Aliaksei Petsiuk
Western University, apetsiuk@uwo.ca

Pierce Mayville
Michigan Technological University, pjmayvil@mtu.edu

Laura Brown
Michigan Technological University, lebrown@mtu.edu

Joshua M. Pearce
Western University, joshua.pearce@uwo.ca

Title page

Monofacial vs Bifacial Solar Photovoltaic Systems in Snowy Environments

Koami Soulemane Hayibo[1], Aliaksei Petsiuk1, Pierce Mayville[2], Laura Brown[3], Joshua M. Pearce[1,4,*]

1. Department of Electrical & Computer Engineering, Western University, Canada
2. Department of Material Science & Engineering, Michigan Technological University, US
3. Department of Computer Science, Michigan Technological University, US
4. Ivey Business School, Western University, Canada
* contact author: joshua.pearce@uwo.ca
1151 Richmond St. N., London, ON, Canada N6A 3K7

khayibo@uwo.ca, apetsiuk@uwo.ca, pjmayvil@mtu.edu, lebrown@mtu.edu, joshua.pearce@uwo.ca

Monofacial vs Bifacial Solar Photovoltaic Systems in Snowy Environments

Abstract

There has been a recent surge in interest in the more accurate snow loss estimates for solar photovoltaic (PV) systems as large-scale deployments move into northern latitudes. Preliminary results show bifacial modules may clear snow faster than monofacial PV. This study analyzes snow losses on these two types of systems using empirical hourly data including energy, solar irradiation and albedo, and open-source image processing methods from images of the arrays in a northern environment in the winter. Projection transformations based on reference anchor points and snowless ground truth images provide reliable masking and optical distortion correction with fixed surveillance cameras. This allows individual PV module-level snow shedding ratio determination as well as average cumulative snow load by employing grayscale segmentation. The data is used to determine the no-snow losses of two systems during summer and snow losses during winter. The results found monofacial snow losses are in average 33% for winter period, and 16% on an annual basis. Bifacial systems perform better than monofacial in severe winter conditions as average winter snow losses was 16% and the annual losses were 2% in the worst-case scenario. In addition, there was a bifacial gain of 19% compared to monofacial system during winter.

Keywords: albedo; bifacial photovoltaics; design optimization; snow; northern environments

1. Introduction

Although historically large-scale solar photovoltaic (PV) projects have consisted of monofacial modules, bifacial modules are rapidly gaining market share [1], as several studies have shown a bifacial gain [2–5]. Bifacial systems have been installed identically to monofacial systems, and thus the minimal additional cost (e.g. ~3%) for bifacial modules is economically attractive [5,6]. The levelized cost-of-electricity (LCOE) calculations [7] shows that solar electricity from bifacial PV has 2–6% lower LCOE than monofacial systems [8]. Trackers have also appeared useful for bifacial deployment [9,10], but additional research is needed to quantify and improve the efficiency, reliability, and configuration of bifacial arrays [11].

The need for additional research is particularly clear in high-albedo settings [12] where little work has focused on bifacial modules, including both artificial environments [13], (e.g. white commercial rooftops [14] or low-concentration substrates [15]), and natural environments (e.g. deserts [16] and snow-covered terrain [17,18]). Regions with substantial snow, may be even more attractive for bifacial PV applications because of the albedo effect. Snow enhanced albedo increases the amount of incident light reflected upward, which is both a primary contributor to general bifacial gain [19,20] and there are some indications that it accelerates snow clearing because of backside surface heating [10]. As more solar projects are installed in snowy environments this has become an area of growing interest [20–23] because it is imperative to properly model snow losses for financing of large-scale PV projects [24–26].

Since snow can completely block the access of solar radiation to the PV panel or module, its presence is an important factor in determining the amount of electricity generated. Poorly designed systems (e.g. those that allow ground interference that prevents snow from sliding off modules can result in double digit annual energy losses [27]). Pawluk et al. [28] presented a literature review on electricity generation loss due to snow, where they identify influencing factors and quantify snow impacts, examine existing assessment methods, and identify mitigation strategies. Wirth et al. [29] introduced a PV system

validation study comparing satellite-based datasets with ground measurements from various meteorological stations. Pelland et al. [30] developed a method for forecasting solar and photovoltaic energy based on the post-processing of a numerical weather prediction model. Lorenz et al. [31] evaluated a snow detection algorithm based on PV power output and meteorological forecast parameters.

Particular attention in the literature is being paid to shading and surface defects detection methods based on computer vision. For example, Afifah et al. [32] provided an overview of image processing techniques for detecting damage on PV panels such as cracking, delamination, discoloration, bubbling, shading, and soiling caused by maintenance, environment, climate, and chemical reactions. Li et al. [33] implemented an automatic defects detection system for large-scale PV installations based on unmanned aerial vehicle inspection and image processing algorithms. The research found in [33] focuses on snail tracks and dust shading segmentation using Gaussian derivative filtering and geometric feature matching. Most relevant PV yield in snowy environments, Andrews et al. [23] validated a methodology for determining snowfall losses from time-series performance data and meteorological observations and developed a method for determining the distribution of snow deposits on solar PV modules from image data. In images captured at five-minute intervals, solar PV arrays are masked, and snow distribution is determined based on grayscale values [23]. Later, Braid et al. [34] developed a method for measuring snow propagation on individual elements of a commercial-scale PV project by applying hue-saturation-value thresholding to transformed images of module sections considered optical distortions. Thus, computer vision is particularly useful for snow-related PV studies.

Non-tracking fixed-tilt solar projects remain the most common type of solar PV system and despite recent efforts, there remains a knowledge gap on the impacts of snow losses for bifacial as compared to monofacial modules for these systems in snowy environments. Many studies have been in the most extreme environments (e.g [22,27]), which do not represent the majority of PV systems found in regions that have some snow losses. To solve this outstanding issue and provide design guidance for those building PV projects in snowy environments, this study analyzes snow losses on these two types of systems using empirical hourly data in a northern environment (Escanaba, MI, USA). The behavior of monofacial and bifacial solar PV systems during winter is investigated. Hourly energy data collected from the inverters is used to analyze the impact of the snow on the energy production of the two systems. Solar irradiation data collected by two pyranometers is analyzed to determine an existing relationship between the albedo and the performance of the two types of system during winter. When analyzing the energy conversion efficiency of solar PV modules, calculations of the amount of snow cover were carried out using open-source image processing methods based on color thresholding and segmentation [35,36]. Projection transformations based on reference anchor points and snowless ground truth images provide reliable masking and optical distortion correction with a fixed surveillance camera. This allows individual PV module-level snow shedding ratio determination by employing grayscale segmentation given image datasets with sufficient contrast. In addition to the above features, the presented research also analyzes the average cumulative snow load for each solar PV module over the entire observation season. The available data is used to determine the no-snow losses of the two systems during summer, and the snow losses during winter. The snow losses analysis results are discussed in the context of designing PV systems for snow-heavy location.

2. Methods

2.1. Escanaba Solar PV System Parameters

The Escanaba solar project is a 1.67 MW(DC) facility is owned by the City of Escanaba, Electric Department. The facility is located adjacent to the Delta County Airport (ESC) with a National Weather Service station (KESC). The project is made up of two systems with one using monofacial PV and the

second using bifacial PV modules for power generation. Both systems are connected to the grid. The monofacial solar PV system is made of 3,510 Canadian Solar monofacial modules of 330 W_{DC} each [37]. The energy generated by the monofacial PV system is injected to the grid through 15 inverters [38], each having a power of 60 kW_{AC}. The total generation power of the monofacial PV system is 1.158 MW_{DC} with a total available inverter power of 0.9 MW_{AC}. On the other hand, the bifacial PV solar PV system has 1,440 Canadian Solar bifacial modules [39], with each module having a power of 355 W_{DC}. The DC power generated by the bifacial PV system is converted into AC power through 6 inverters 65 kW_{AC} each [40], amounting to a total inverter power of 0.39 MW_{AC} and a total DC generation power of 0.511 MW DC. Figure 1 displays a top view of the system showing the monofacial and bifacial arrays of modules.

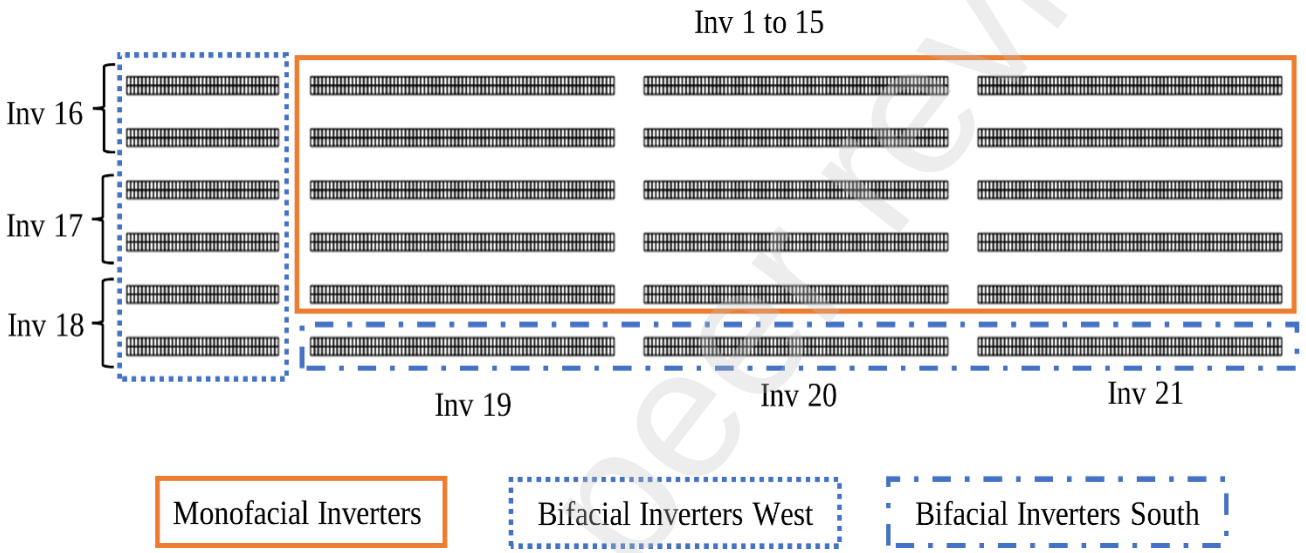

Figure 1. Bird's eye view of the layout of the system. The monofacial panels are within the solid line; and the bifacial panels are within the dashed line for the system arranged on the west and dash-dot line for those arranged in a line facing south.

2.2. Energy Generation and Snow Loss Analysis

A comparative energy generation analysis is performed between the two PV systems. The goal of the analysis is to determine the increase in energy production in the bifacial system as compared to the monofacial (bifacial gain), especially in winter. The analysis period runs from November 1, 2020, to September 30, 2021. The power generated by the PV project is recorded with a time resolution of 1-minute and aggregated into an hourly-based power value for each inverter individually. The data was cleaned and processed using Python and Google Colab [41]. The preliminary exploration of the data has shown that one of the inverters of the bifacial system has recorded 7000 less data points due to equipment failure and an extended outage waiting on a warranty replacement. Therefore, that specific inverter 16 was not considered during the energy analysis. Also, Figure 2 shows that there is a discrepancy between the missing data points across the remaining inverters. The average number of missing data 3,515 represent mostly nighttime records when the sun was down, and the system was not producing energy. All the rows containing missing data were dropped to ensure no inverter had more weight in the analysis than the others. The parameters of the system with inverter 16 dropped are shown in Table 1.

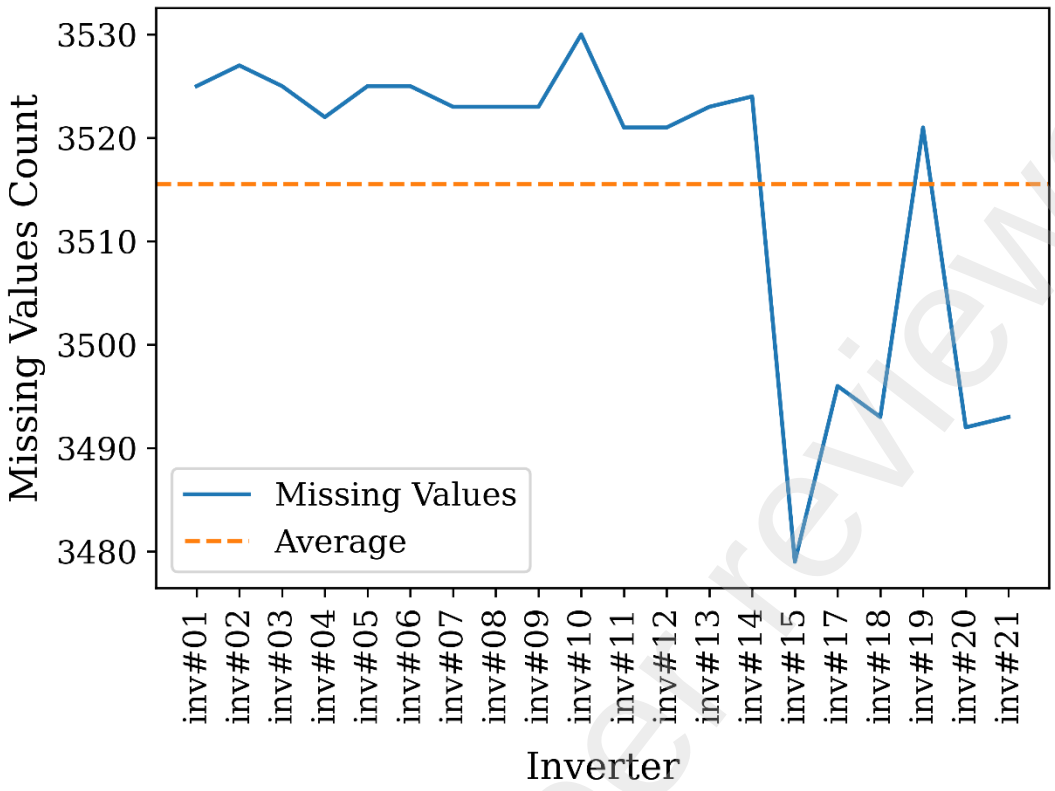

Figure 2. Count of missing values for all inverters except inverter 16, one of the bifacial system inverters.

Table 1. Parameters of the Escanaba Solar Project after removing an inverter of the bifacial system.

	Monofacial System	**Bifacial System**	**Escanaba Solar Project**
Number of Solar Modules	3,510	1192	4,702
DC Power per Module (Wp)	330	355	-
DC Capacity of the System, (MWp)	1.158	0.423	1.581
Number of Inverters	15	5	20
Power of an Inverter (kW_{AC})	60	65	-
Theoretical Percent Contribution (%)	73.24	26.76	100

The hourly power generation P_h (W) in each case is aggregated into a daily energy generation E_d (Wh) for each inverter (see equation (1)). Then, the total generation is computed for the monofacial and the bifacial system. Because the two systems have different DC generation power and utilize different inverters, the analysis is performed using the specific yield of both systems. The specific yield E_y (kWh/kW_{DC}) in both systems is calculated by dividing the energy production by the nameplate DC power of the system P_{DC} (kW_{DC}) as shown in equation (2). In the case of the bifacial system the total DC power does not include inverter 16.

$$E_d = \sum_{day} P_h \quad \text{(Wh)} \qquad (1)$$

$$E_y = E_d / P_{DC} \quad (\text{kWh/kW}_{\text{DC}}) \quad (2)$$

When all the components of the solar PV project are operating normally (without inverter 16), the overall system has a DC capacity of 1.581 MW_{DC}, where the monofacial system's power is 1.158 MW_{DC} and the power of the bifacial system is 0.423 MW_{DC}. As a result, the theoretical percent contribution of the monofacial system is 73.24% and the theoretical percent contribution of the bifacial system is 26.76%. If both systems were operating normally throughout the study period, it can be inferred that these percent contributions would be the same in terms of their recorded energy production. On this basis, the evaluation of the percent contribution of the real time daily energy production and the theoretical energy production, provides useful information about the system's behavior. The actual percent contribution $(PC)_{bifacial}$ (%) of the bifacial system is calculated by dividing the bifacial system energy generation by the combined generation of the two systems (equation(3)).

$$(PC)_{bifacial} = \frac{E_{bifacial}}{E_{bifacial} + E_{monofacial}} \times 100 \quad (\%) \quad (3)$$

The percent contribution of the bifacial system is compared to the albedo at the location of the project. The albedo data is derived from two Apogee pyranometers [42] installed at the project. The first pyranometer, facing upwards towards the sky, measures the direct solar irradiation I_d (W/m^2) or the downward irradiation. The second pyranometer, facing downwards towards the ground, captures the reflected solar irradiation I_r (W/m^2) or the upward shortwave irradiation. The two pyranometers were set up to have a time resolution of 30 minutes. The internal clocks of the pyranometers did not correspond to the sunlight hours of Escanaba and were not synchronized. Therefore, the data recorded by each pyranometer was corrected by aligning the first measurement captured each day with the sunrise time obtained from a National Center for Environmental Information (NCEI) database [43]. After cleaning and aligning the data, the 30-minute albedo α_{30mn} is calculated by dividing the upward radiation by the downward radiation (see equation (4)). The 30-minute albedo data has then been aggregated to calculate a daily albedo α_{daily} using a weighted average as shown in equation (5) [44]:

$$\alpha_{30mn} = I_r / I_d \quad (4)$$

$$\alpha_{daily} = \frac{\sum_i (I_{d_i} \times \alpha_{30mn_i})}{\sum_i I_{d_i}} \quad (5)$$

The energy generation data, the pyranometer data, as well as additional weather data obtained from Solcast [45] were used to determine the snow losses of the two systems during the winter period. The System Advisor Model (SAM) [46], developed by the U.S. National Renewable Energy Lab (NREL) was used to perform the energy simulation. Three models were built in SAM for the two systems using the specifications in Table 1 as well as the exact electrical and geometrical configuration of the systems. Two of the models were used to describe the bifacial system, west and south as shown in Figure 1. The detailed parameters of the models are stored in an open-source repository [47]. The models are built for a single inverter in each system.

A first simulation was run for July 4 and July 5, 2021, using measured pyranometer irradiation data. During this first simulation, all the losses were set to zero in SAM. The resulting energy production was

compared to the actual energy generated by the system during July 4 and July 5, 2021. The energy deficit between the simulation value and the real value is used to determine the actual system losses. Since the simulation is performed for the month of July, which is a summer month, the system losses obtained are snow-free losses. In the second simulation, the losses in SAM were set to the calculated snow-free losses value, and weather file obtained from Solcast was used to evaluate the theoretical energy of the system during the winter period. Finally, the theoretical energy obtained in SAM during the winter period was compared to the actual energy produced during the same period to determine the winter snow losses of the monofacial, and the bifacial systems, respectively.

2.3. Snow Coverage from Image Analysis

The analysis period was from 11/01/2020 to 03/31/2021. Images of the monofacial and bifacial solar PV modules were captured independently by two cameras at approximately 15-minute intervals. Pictures taken at night were not used for analysis due to insufficient lighting. Thus, during the day, 32 images were generated for each PV module, characterizing the state of the snow cover from 9:00 in the morning to 17:00 in the evening. A total of 4,826 images were analyzed for each PV module for the specified period.

Figure 3 shows reference images of the solar PV modules and their unwrapped active surfaces with masked solar pads. Snow segmentation and determination of the size of the snow cover boundaries were carried out individually for each solar PV module's active area. Due to lens distortions, PV module images appear warped. To compensate for this curvature and to segment solar PV module's active area, ground truth images taken on a snowless day were selected for each PV module. The dark color of the PV module's active area contrasts well with the surrounding metal frame, which makes it possible to apply a grayscale threshold for their segmentation.

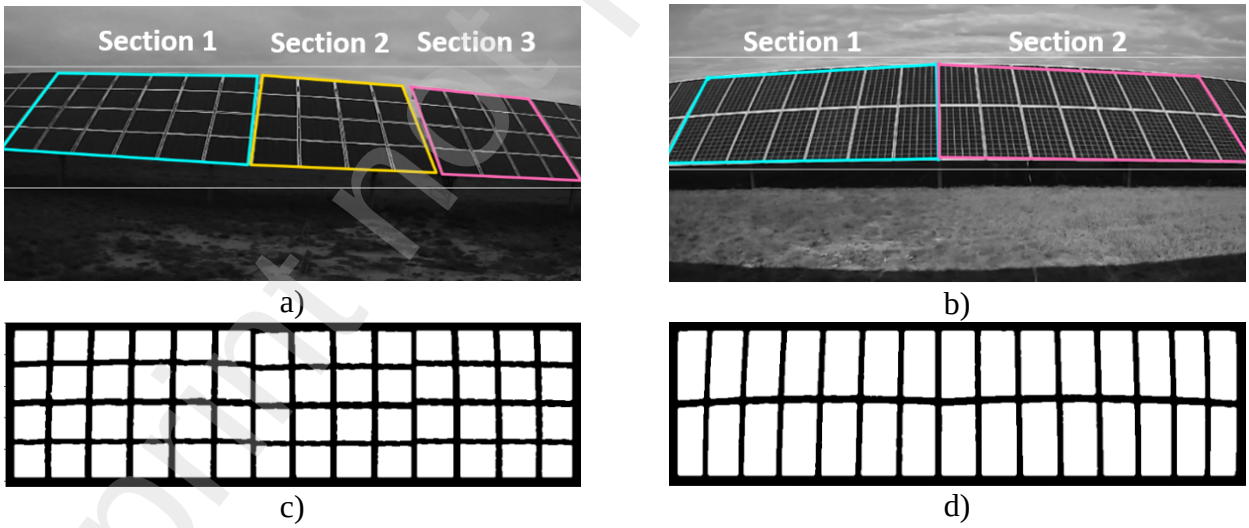

Figure 3. Reference images of the solar PV module groups and their unwrapped active surfaces. The colored outlines mark the sections of the PV modules that are closest in shape to the parallelograms. *a)* reference image of the bifacial solar PV module, *b)* reference image of the monofacial solar PV module, *c)* unwrapped active surface of the bifacial PV module with 56 masked square solar PV module's active areas, *d)* unwrapped active surface of the monofacial PV module with 30 masked rectangular solar PV module's active areas

Since both cameras are stationary, the virtual unfolding of the PV modules is carried out based on the reference corner points of the section boundaries, which are close in shape to parallelograms. For the bifacial PV array, three sections were defined, consisting of 6x4, 4x4, and 4x4 small square solar PV module active areas, respectively. The monofacial PV module array, in turn, consists of two sections with 7x2 and 8x2 rectangular solar PV module active areas. Each section virtually unfolds using the perspective transforms of the OpenCV library [48]. The unwrapped sections of each PV module were combined into a common region, and the resulting masks were used for the entire image dataset (Figure 3).

PV module size was measured in relative units. Thus, the dimensions of the bifacial PV module, consisting of 56 individual PV module active areas, are 916x260 pixels, and the dimensions of the monofacial PV module, consisting of 30 rectangular PV module active areas, are 920x260 pixels. The solar PV module active area of both PV modules are then masked to exclude the metal frame from the snow segmentation.

Figure 4 depicts the process of snow segmentation and determination of the solar PV module overlap percentage. The given method is based on grayscale thresholding due to the high contrast of the snow compared to the dark background of the solar PV. The amount of snow overlap is determined by the ratio of the snow area to the area of the entire solar PV module. In addition, a snow load map was calculated for each PV module type, which clearly shows the solar PV with the greatest snow coverage.

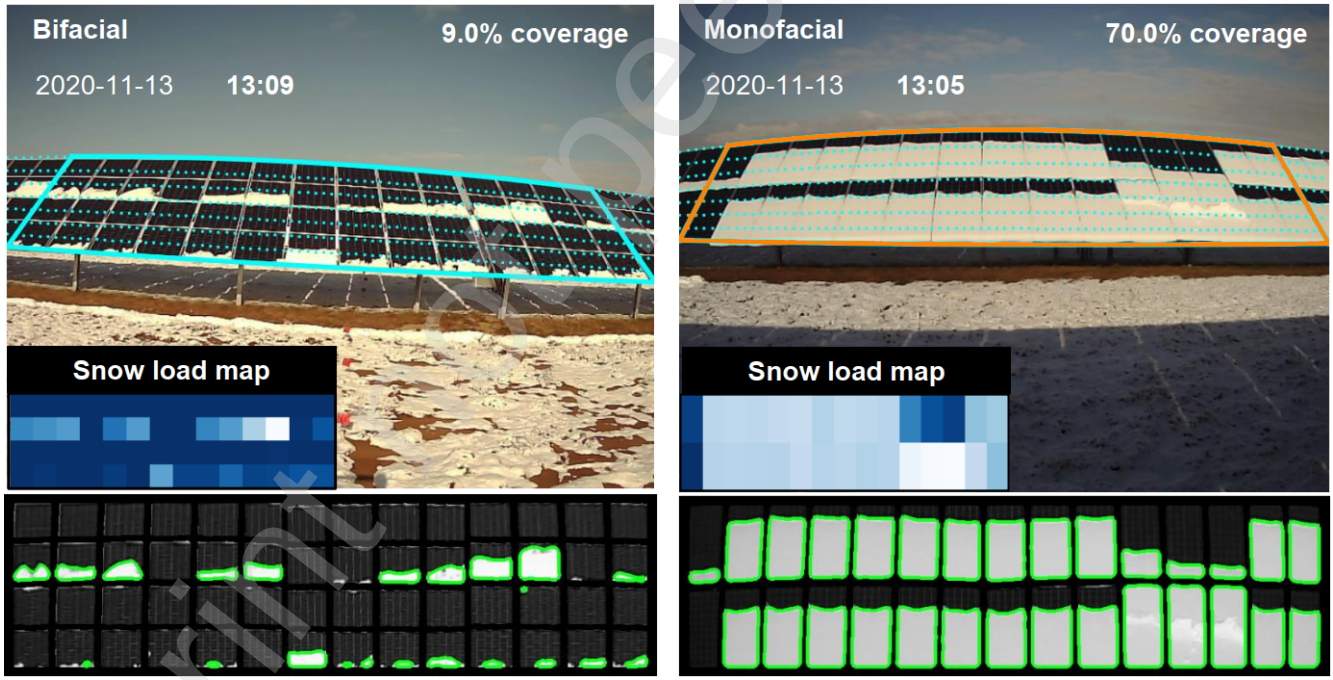

Figure 4. Snow segmentation and determination of solar PV module overlap percentage.

The average snow shading for each day is determined by summing the segmented snow coverages for each image and dividing the resulting snow load by the total number of images acquired to date. This allows leveling out minor segmentation errors for each individual image.

Finally, maps of averaged cumulative snow load were calculated for the entire winter analysis period for each PV module.

3. Results

3.1. Energy Generation Results

For the energy generation analysis in this study, the period of interest is split into two, a winter period running from November 30, 2020, to March 4, 2021, which is the period with snow, and a non-winter period spanning between March 5, 2021, to September 30, 2021, when the weather has no snow. The daily energy production profile of the project is shown in Figure 5 for the entire period of the study. As expected, the overall energy generated by the monofacial system is higher than the energy generated by the bifacial system, because the DC power of the monofacial system is overall higher compared to the bifacial. The energy yield in Figure 5 shows that both systems have similar energy yield values, and the energy yield is higher during the winter period as compared to the non-winter period.

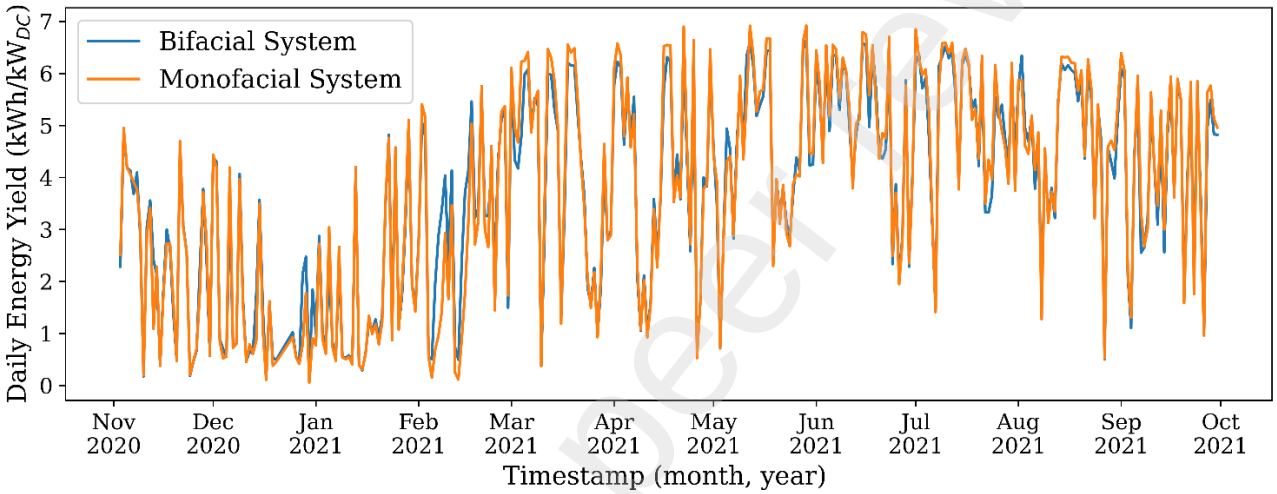

Figure 5. Energy yield profile (kWh/kW$_{DC}$) of the monofacial system and the bifacial system, the box shows the winter period.

Figure 6 compares the monthly energy yield of the solar project for the months of February 2021 and July 2021. These two months have been chosen as characteristics month for the winter and non-winter periods, respectively. Because there is no snow on the modules in July, the month of July is considered as the base case operation of the project. On Figure 6a, the energy yield of all the inverters (monofacial and bifacial) is between 140 kWh/kW$_{DC}$ and 160 kWh/kW$_{DC}$. Also, Figure 6a, shows that there is no significant difference between the energy yield of the monofacial system and the bifacial system, validating the results shown in Figure 5. This result is unexpected because of previous work. The bifacial system should theoretically have a higher yield compared to the monofacial and is discussed further in Section 4**.** On the other hand, during February, all the panels do not perform equally. The bifacial system has a clearly superior performance compared to the monofacial system. The lowest performing bifacial inverter has a similar yield (86.1 kWh/kW$_{DC}$) as the highest performing monofacial inverter (85.7 kWh/kW$_{DC}$). The bifacial system performs as high as 95.3 kWh/kW$_{DC}$ while the monofacial performs as low as 66.1 kWh/kW$_{DC}$. Figure 6b also reveals that there is a divergence between the yield of the inverters both monofacial and bifacial during the winter period. This is correlated with the findings of the snow coverage analysis.

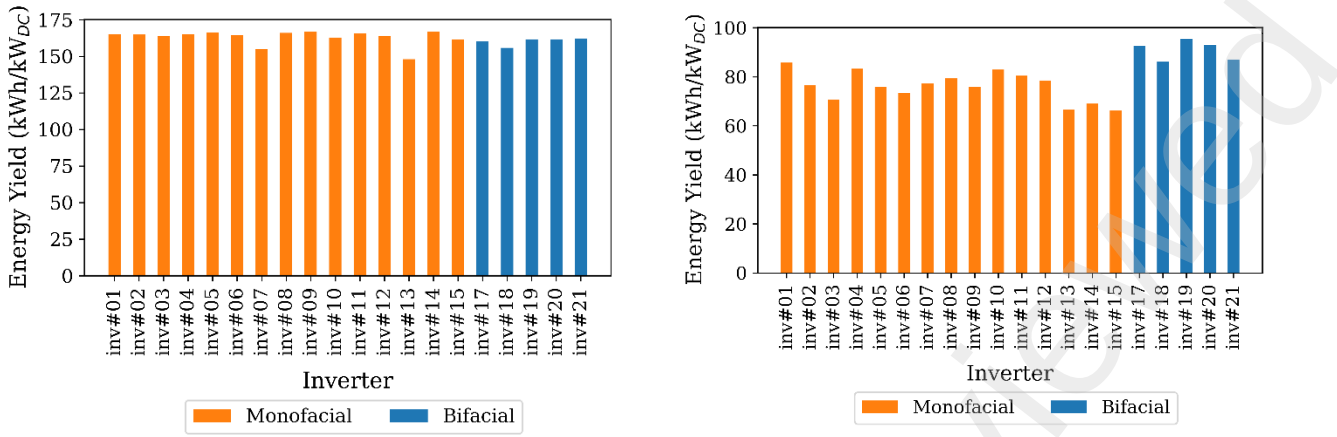

(a) July 2021

(b) February 2021

Figure 6. Detailed energy yield of all the inverters in the project for the two characteristic months. (a) July 2021. (b) February 2021.

Figure 7 shows the hourly result of the percent contribution calculation. The baseline plot on Figure 7 and Figure 8 represent the theoretical percent contribution (26.76%) of the bifacial system calculated using the power output of both systems. On Figure 7a, the delimitation between the winter and non-winter behavior of the plant is clearly shown. When the percent contribution is at the baseline percentage, the two systems are performing as predicted. This means that the bifacial system's contribution to the overall system is 26.76% while the contribution of the monofacial is 73.24%. On the other hand, when the percent contribution of the bifacial system is above the baseline, then the bifacial system is contributing more than the theoretical contribution of 26.76%. Similarly, when the percent contribution is below the baseline, the monofacial system is contributing more than 73.24%. According to Figure 7a, the bifacial system's production is higher than the monofacial system's production during the winter period. For a detailed analysis of the percent contribution data, histograms of the winter period and the summer period are plotted on Figure 7b and Figure 7c, respectively. Figure 7c shows a normal-like distribution centered around the baseline percentage of the bifacial system (26.76%). The normal-like distribution confirms that both systems have similar yields during the non-winter period. The plot on Figure 7b shows a bimodal distribution for the winter period. The first part of the distribution is normal and centered at the baseline percentage while the second part is uniform at 100%. This bimodal distribution indicates that the project has two different behaviors during winter. This observation infers that the modules behave differently during winter depending on whether they are covered by snow or not.

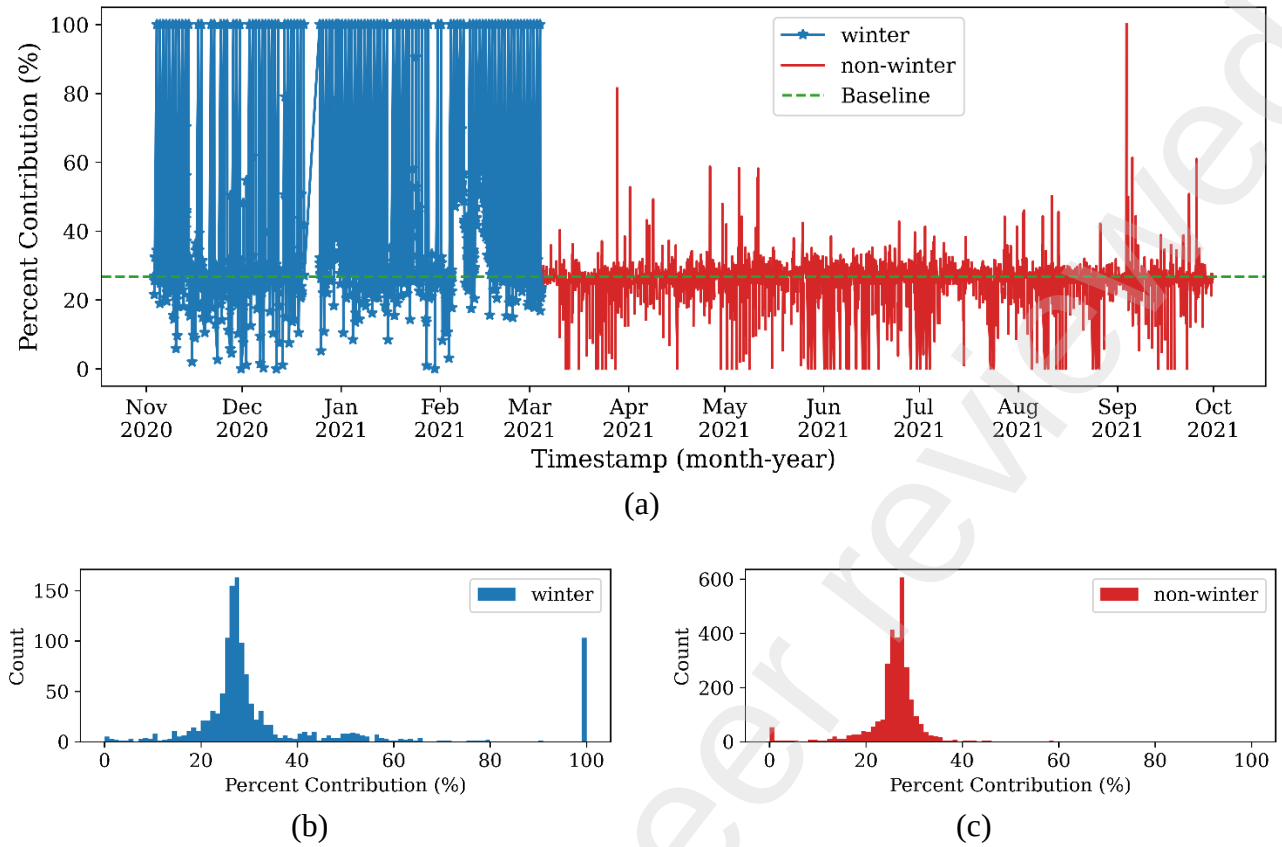

Figure 7. Hourly results of the percent contribution (%) calculation for the bifacial system. (a) Hourly representation of the percent contribution during the winter period and the non-winter period. (b) Distribution of the percent contribution during the winter period. (c) Distribution of the percent contribution during the non-winter period.

The pattern observed in the percent contribution on an hourly basis is also reflected when the data is the daily percent contribution. Figure 8 shows that for the winter months, especially, November, December, and February, there are peaks in the percent contribution, and these peaks correspond to the days with the highest snowfall of the study period [49].

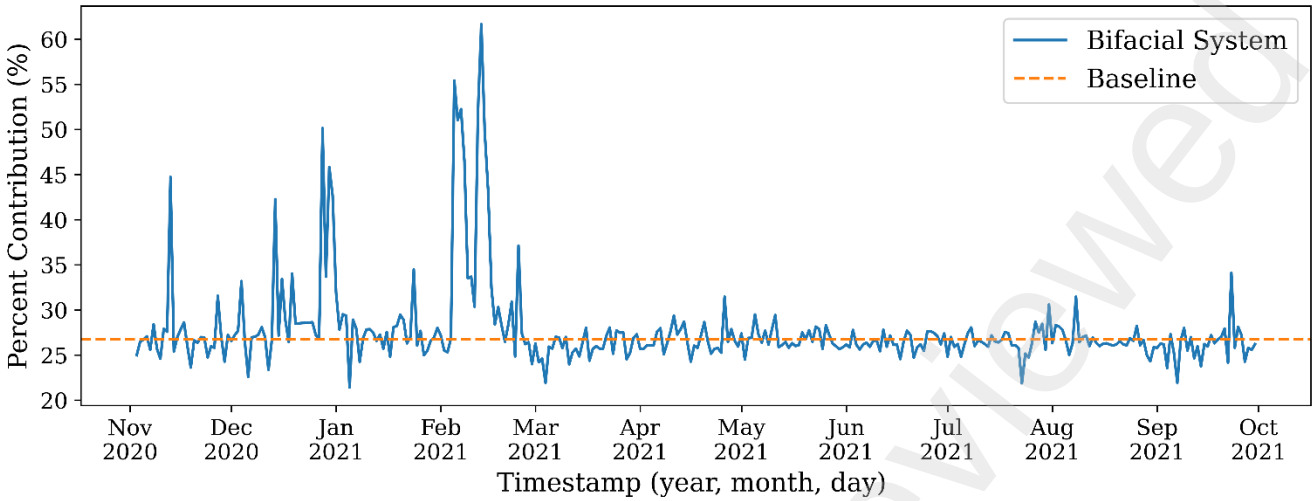

Figure 8. Daily percent contribution (%) of the bifacial system energy production during the analysis period compared to its theoretical baseline contribution of the bifacial system.

In Figure 9a, the albedo is compared to the percent generation contribution of the bifacial system. Both plots appear to follow a pattern, therefore the albedo is scatter-plotted against the percent contribution and the energy yield of the bifacial as shown on Figure 9b and Figure 9c, respectively. Figure 9b shows an exponential relationship between the albedo and the percent contribution. Nevertheless, this observation is biased since the relationship is only observed during winter. On the other hand, Figure 9c shows no correlation between the albedo and the energy yield of the bifacial system.

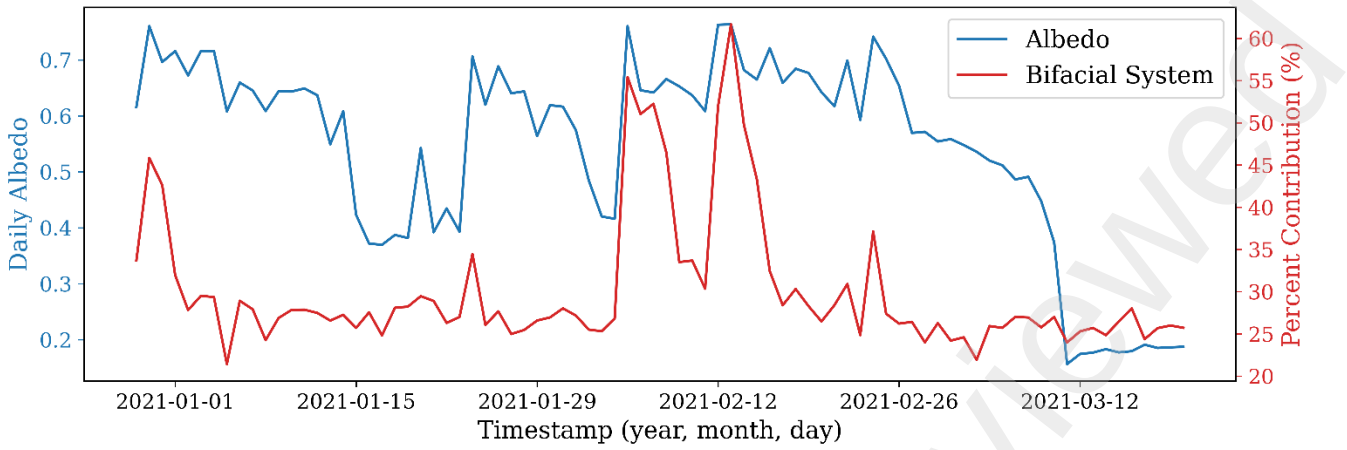

(a)

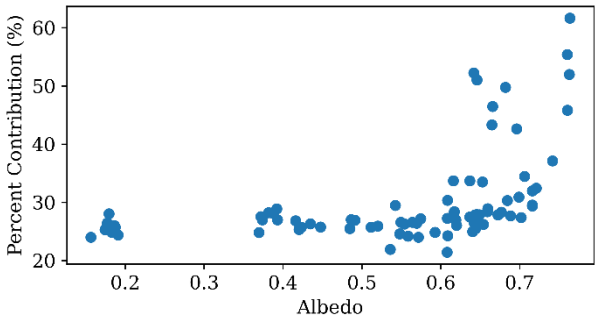

(b) December 29, 2020 to March 19, 2021

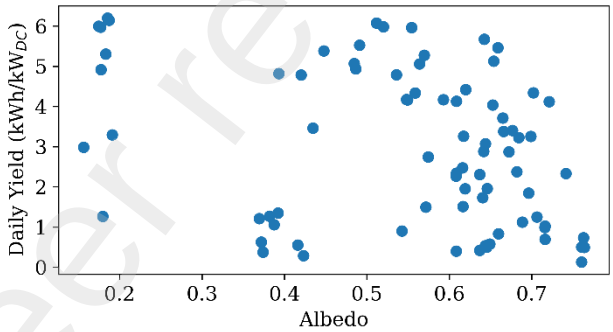

(c) December 29, 2020 to March 19, 2021

Figure 9. Results of the daily albedo analysis. (a) Representation of the daily albedo and the percent generation contribution (%) of the bifacial system between December 29, 2020, and March 19, 2021. (b) Scatter plot of the albedo and the percent contribution of the bifacial system. (c) Scatter plot of the albedo and the daily energy yield (kWh/kW$_{DC}$) of the bifacial system.

Figure 10 displays the boxplot of the snow losses during the winter. It should be specified that the losses plotted on Figure 10 are the losses due only to snow covering the surface of the modules in the monofacial and bifacial systems. The results clearly show that the monofacial system has a lower performance during the winter when the modules are covered in snow. The average snow losses in the monofacial system are 33.12% with a maximum value of 36.41%, and a minimum value of 30.63%. In contrast, both the bifacial subsystems (south and west bifacial arrays) have snow losses below 18%. The average snow losses for the bifacial subsystem located to the west are 14.90%, with a maximum and minimum value of 17.52% and 12.27% respectively. The maximum and minimum snow losses for the south bifacial subsystem are 16.28% and 16.03% with an average value of 16.20%.

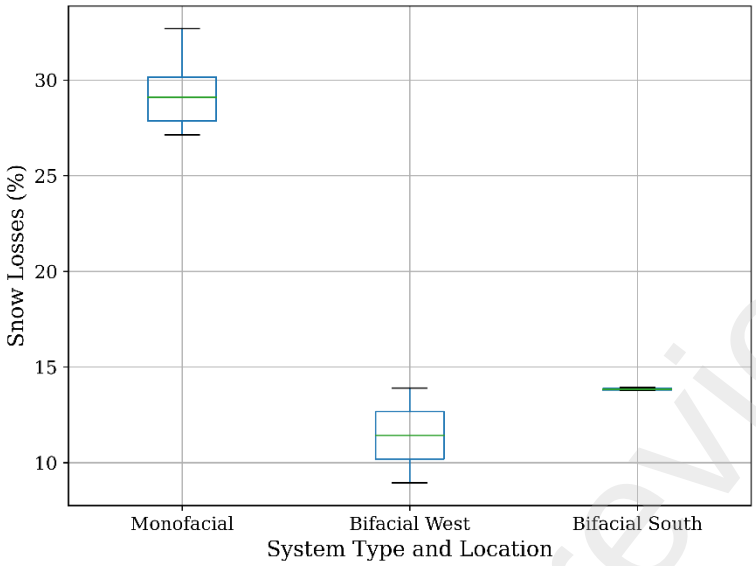

Figure 10. Snow losses boxplot during the winter (November 1, 2020, to March 4, 2021) for the monofacial system and the bifacial system.

When the method used to calculate the winter snow losses is applied to the entire study period (November 1, 2020, to September 30, 2021), the average annual snow losses for the monofacial system is 16.37%, while the average annual snow losses for the bifacial south and west subsystems are 2.24%, and 0.24%, respectively.

3.2. Snow Coverage Results

The daily amount of snow shading on the monofacial and bifacial PV modules is shown in Figure 11.

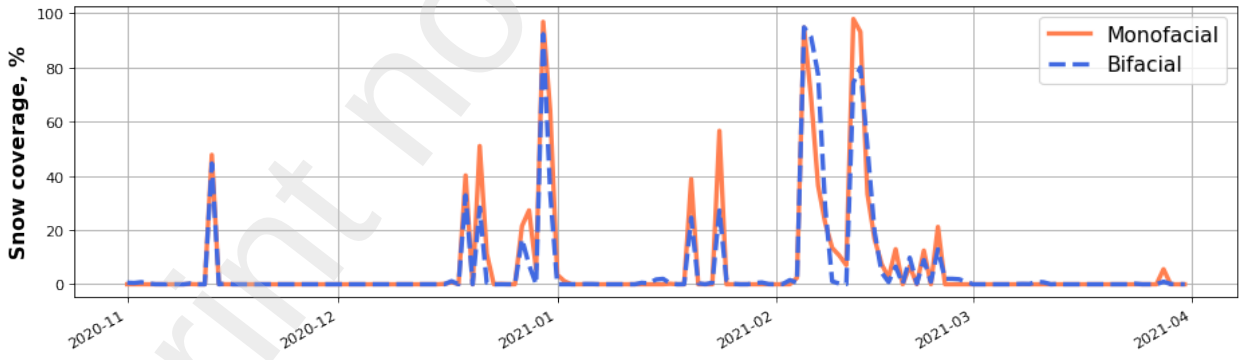

Figure 11. Daily amount of snow (from 9:00 am to 17:00 pm) on the monofacial and bifacial solar PV modules

Figure 12 shows the difference in the percentage of snow cover for both monofacial and bifacial PV module arrays. Over the entire observation period, the total shaded area of the monofacial PV system is approximately 1.15 times larger than the total shaded area of the bifacial PV system. The observation period lasted 151 days, about 30 of which were during periods of snowfall. In total, for approximately two-thirds of the snowfall period, the monofacial module array had a greater snow load than the bifacial one (Figure 12 Figure). In most cases, after the snowfalls, the bifacial PV module clears more rapidly.

This has previously been hypothesized to be from back surface heating, which causes the snow to slide off the bifacial modules more rapidly as a layer of water decreases the sticking coefficient for snow on the module [10]. Typical snow shading dynamics over several days with the 15-minute temporal resolution is shown in Figure 13 and confirm this hypothesis. This observation, however, does not prove this phenomenon has systematic nature.

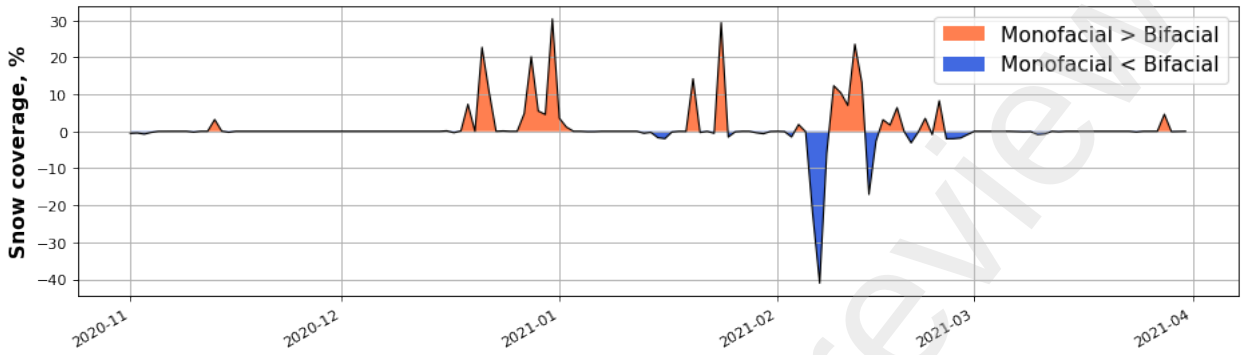

Figure 12. Difference in the percentage of snow cover for monofacial and bifacial PV modules

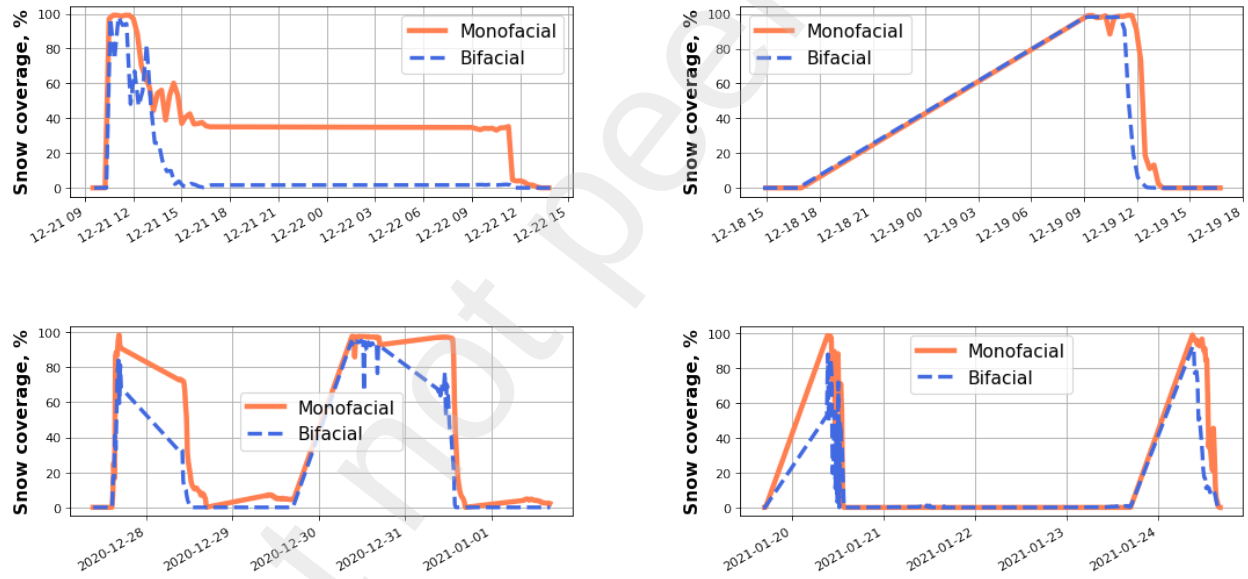

Figure 13. Typical snow shading dynamics over several days with the 15-minute temporal resolution

In addition, maps of averaged cumulative snow load were calculated for the entire analysis period for each PV module (Figure 14). Thus, certain areas of the solar PV modules are more loaded with snow than others during the entire winter season. This information can be used in the future to develop adaptive heating or snow removal systems.

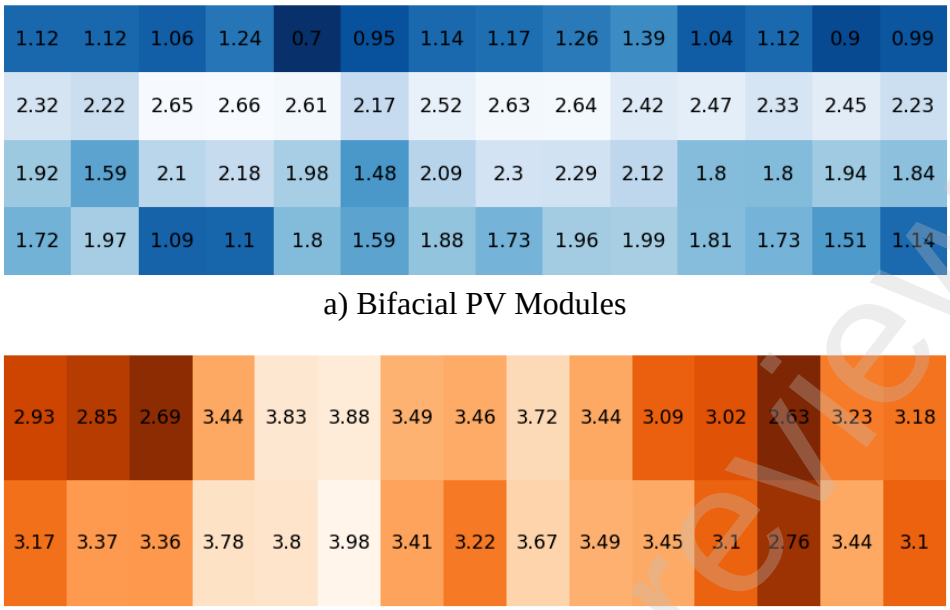

a) Bifacial PV Modules

b) Monofacial PV Modules

Figure 14. Average snow load map for the bifacial PV modules (blue) and monofacial PV modules (orange). Each cell represents individual solar PV module's active area with an average cumulative snow load as a percentage of the load of the entire module.

4. Discussion

The energy production and image analysis performed in this study have shown that a bifacial PV system performs better in a snowy environment compared to a monofacial PV system. Both systems have similar yields during periods with no snow (March 5, 2021, to September 30, 2021), but the bifacial system's yield outperforms its monofacial counterpart during the winter (November 1, 2020, to March 4, 2021). The bifacial system's lowest yield during winter (86.1 kWh/kW_{DC}) surpasses the monofacial system's yield (85.7 kWh/kW_{DC}) during the same period. There is an exponential relationship between the albedo and the overall percent contribution of the bifacial system. The snow loss analysis has shown that the bifacial system only loses 0.24% to 2.24% of its annual energy due to snow coverage, while the monofacial system loss in average is 16.37%. The snow coverage analysis using computer vision has shown the bifacial system having a faster snow clearing rate than the monofacial PV system.

The average winter snow losses (33.12%) and the annual losses due to snow (16.37%) for the monofacial system are in agreement with the results obtained in previous work for severe winter climate locations [28]. The average winter generation losses for a location that have a similar annual snowfall profile as Escanaba, were estimated between 13% and 68%, depending on the inclination angle while the annual electricity generation losses were between 5% and 34% [27,28,50]. On the other hand, the average snow losses from the bifacial system according to the results of the present study are lower than 2.5%. This result is corelated to the bifacial energy yield gain observed during winter.

During February, the characteristic winter month for the study, the bifacial system has an average energy yield of 90.82 kWh/kW_{DC}, and the monofacial system's average energy yield is 76.12 kWh/kW_{DC}. As a result, the bifacial gain during the characteristic winter month of February is 19.31%. The bifacial gain is explained further by exploring the results of the computer vision analysis. According to the camera

image analysis, the snow on the bifacial modules surface clears faster than the monofacial modules. Even though this observation seems to not have a systematic nature on its own, when it is combined with the energy yield, albedo and snow losses results, the bifacial modules have a net energy production advantage compared to the monofacial system. Furthermore, even though there is no direct relation between the energy yield and the albedo (see Figure 9c), the scatter plot on Figure 9b confirms that the bifacial gain is linked to the albedo increase during winter. The higher the albedo, the higher the bifacial gain, and the lower the snow coverage on the bifacial as compared to the monofacial system (see Figure).

The energy yields of the two systems are similar except for the winter days where the bifacial system has a better yield than the monofacial system. Theoretically, the yield of the bifacial system would be greater than the monofacial system during the entire period of study [14,51,52]. This is because the type of module used in the monofacial and the bifacial have similar peak DC power on the front surface, and the bifacial modules have an additional energy capture surface at the back. Nevertheless, because of the geometry of the project (see Figure 1), the back surface of the bifacial modules appears to not receive the substantial reflected solar energy in low albedo conditions. The discrepancy that derives from the geometry of the system is explained by the difference between the snow losses of the west and south bifacial subsystems. The losses of the inverters in the bifacial subsystem located to the south have a small standard deviation (0.14) while the stand deviation of the losses of the west inverters are 3.70 as displayed in Figure 10. A possible explanation of this observation is the geometry and the spacing between the rows of the plant. Even though the spacing is optimized for the monofacial system, it is not optimized for the reflected light to reach the back of the modules in the system, especially in summer. This could explain why there is a uniformity in the losses observed throughout the bifacial inverters located to the south of the plant while the losses of the west bifacial inverters have a high variability. There is a compound shading effect, not on the front surface of the modules, but at the rear of the module that curbs down the energy generated by the bifacial system in summer. This shading effect is overcome during winter by the high value of the albedo of snow on the ground. As a result, the findings in this study relating to the snow losses of the bifacials system are conservative values. This draws a particular attention to the need for further optimization of the layout design of a solar PV project using bifacial modules.

According to these observations, the interrow spacing in bifacial PV systems needs to be increased during the design phase to allow for reflected solar radiation to reach the back of the modules, and future work is required to explore the optimal layout design of a PV project combining monofacial and bifacial modules. Previous studies have shown that snow clearing on solar PV modules is accelerated in frameless modules [53,54]. Combining frameless technology and bifacial PV modules offers an opportunity to enhance snow shedding in bifacial systems in wintery environments. This is a promising alternative that should be investigated further both from an industry perspective and a research perspective. Another parameter that highly influences snow shedding in solar PV modules is the tilt angle [27,28,50]. In this study the tilt was fixed at 35°, future studies are needed to investigate the bifacial gain and snow losses in higher latitudes and severe snow climate for different tilt angles at the same latitude. It should also be pointed out that while snow losses are important now, as the climate changes the expected snow losses over a PV systems lifetime provide less and less of an impact [55].

A recent study has shown that the use of shotcrete as photovoltaic racking could reduce the cost of PV racking at higher latitudes if the existing PV systems could generate at least 18 % more energy [15]. The bifacial gain obtained in this study (19.31 %), complements the shotcrete study, but requires a new racking geometry as the earlier study was for monofacial PV and allowed for no albedo gathering on the back side. Through the fact that the energy increase obtained because of the high albedo of the snow is just as high as the value required for the use of shotcrete. Also, using shotcrete around bifacials PV

racking offers the possibility to coat the shotcrete racks in superhydrophobic [56] material that would increase the albedo of the surface, providing an opportunity to increase the bifacial gain throughout the whole year. Futures studies are needed to conduct a detailed analysis of the impact of combining shotcrete reflectors or other high albedo materials with bifacial systems on the cost of the racking of the system, and consequently the levelized cost of electricity. This can be further expanded to other type of high reflective surfaces such as white sand, or high albedo plants (offering the possibility of exploring bifacial gain in agrivoltaic systems), especially with the use of back reflectors for bifacials to compliment reflector technologies used for the front surface of PV modules [57,58].

The open-source methods for image analysis are the most sophisticated to date but could be improved. In the future, the developed surveillance system can be improved by adding near-infrared and shortwave infrared channels [59]. Additionally, an RGB color space transformation can be applied for more reliable segmentation in conditions with strong reflections or shadows [60].

5. Conclusions

In this study, bifacial and monofacial PV modules energy yield and snow losses are analyzed in a severe winter climate. The analysis is performed using a combination of empirical recorded hourly data analysis and simulation. Data was recorded through the system's inverters, a pair of pyranometers, and a set of cameras, and was analyzed using data analysis techniques and open-source computer vision. The energy yield analysis has shown that the bifacial modules performed better than the monofacial, especially during the winter period, yielding a bifacial gain of 19.31 % during the characteristic winter month. The computer vision analysis combined with the observed correlation between the albedo and the energy gain provided by the bifacial system have shown that the bifacial system might clear snow faster than the monofacial system. The snow losses analysis has revealed that the bifacial performs better than the monofacial system in winter, as well as on an annual basis. The annual snow losses of the monofacial system were on average 16.37 % while the bifacial system only lost between 0.24 and 2.24 % of its annual energy production due to snow. Even as utility power density on utility-scale solar projects increases, this study has revealed the importance of carefully designing the interrow spacing of solar plants involving bifacials modules. These results show the benefit of using bifacial systems in severe winter climate, and in location with albedo in general, to improve the overall performance of solar PV plants.

6. Conflicts of interest

The authors declare no conflicts of interest

7. Acknowledgments

This work was funded by the Witte and Thompson endowments as well as the U.S. National Science Foundation Convergence program, on a project titled "GCR: Michigan Community & Anishinaabe Renewable Energy Sovereignty [MICARES]," award #1934346. The authors would also like to thank Solcast for supporting this research.

8. References

[1] Wood Mackenzie, Wood Mackenzie (2019).

[2] T.S. Liang, M. Pravettoni, C. Deline, J.S. Stein, R. Kopecek, J.P. Singh, W. Luo, Y. Wang, A.G. Aberle, Y.S. Khoo, Energy Environ. Sci. 12 (2019) 116–148.

[3] R. Kopecek, J. Libal, Nat Energy 3 (2018) 443–446.

[4] I. Shoukry, J. Libal, R. Kopecek, E. Wefringhaus, J. Werner, Energy Procedia 92 (2016) 600–608.

[5] J.S. Stein, D. Riley, M. Lave, C. Hansen, C. Deline, F. Toor, in: 2017 IEEE 44th Photovoltaic Specialist Conference (PVSC), IEEE, Washington, DC, 2017, pp. 3184–3189.

[6] J. Appelbaum, Renewable Energy 85 (2016) 338–343.

[7] K. Branker, M.J.M. Pathak, J.M. Pearce, Renewable and Sustainable Energy Reviews 15 (2011) 4470–4482.

[8] W. Gu, T. Ma, S. Ahmed, Y. Zhang, J. Peng, Energy Conversion and Management 223 (2020) 113283.

[9] A. Di Stefano, G. Leotta, F. Bizzari, in: 33rd European Photovoltaic Solar Energy Conference and Exhibition EUPVSEC, 2017, pp. 1978–1982.

[10] L. Burnham, D. Riley, B. Walker, J.M. Pearce, in: 2019 IEEE 46th Photovoltaic Specialists Conference (PVSC), IEEE, Chicago, IL, USA, 2019, pp. 1320–1327.

[11] R. Guerrero-Lemus, R. Vega, T. Kim, A. Kimm, L.E. Shephard, Renewable and Sustainable Energy Reviews 60 (2016) 1533–1549.

[12] R.W. Andrews, J.M. Pearce, Solar Energy 91 (2013) 233–241.

[13] M.P. Brennan, A.L. Abramase, R.W. Andrews, J.M. Pearce, Solar Energy Materials and Solar Cells 124 (2014) 111–116.

[14] W. Muehleisen, J. Loeschnig, M. Feichtner, A.R. Burgers, E.E. Bende, S. Zamini, Y. Yerasimou, J. Kosel, C. Hirschl, G.E. Georghiou, Renewable Energy 170 (2021) 613–619.

[15] M.R. Hollman, J.M. Pearce, Solar Energy 216 (2021) 386–395.

[16] A.A.B. Baloch, S. Hammat, B. Figgis, F.H. Alharbi, N. Tabet, Renewable Energy 159 (2020) 50–63.

[17] M. Lewis, C. Valdivia, C. Tu Li, A. Russel, H. Schriemer, K. Hinzer, (2018).

[18] M.T. Bembe, S.P. Daniel Chowdhury, N. Meeding, E.G. Lekhuleni, M.B. Ayanna, S. Simelane, in: 2018 IEEE PES/IAS PowerAfrica, IEEE, Cape Town, 2018, pp. 734–738.

[19] Y. Taomoto, K. Hosokawa, M. Yagami, H. Hanzawa, T. Ohkawa, K. Iwamoto, (2016).

[20] W.F. Marion, Albedo Data to Facilitate Bifacial PV System Planning, National Renewable Energy Laboratory, Albuquerque, NM, USA, 2019.

[21] R.W. Andrews, J.M. Pearce, in: 2012 38th IEEE Photovoltaic Specialists Conference, IEEE, Austin, TX, USA, 2012, pp. 003386–003391.

[22] T. Townsend, L. Powers, in: 2011 37th IEEE Photovoltaic Specialists Conference, IEEE, Seattle, WA, USA, 2011, pp. 003231–003236.

[23] R.W. Andrews, A. Pollard, J.M. Pearce, Solar Energy 92 (2013) 84–97.

[24] S. Hosseini, S. Taheri, M. Farzaneh, H. Taheri, IEEE Trans. Ind. Electron. 65 (2018) 7975–7983.

[25] B. Hashemi, A.-M. Cretu, S. Taheri, IEEE J. Photovoltaics 10 (2020) 1044–1052.

[26] M. van Noord, T. Landelius, S. Andersson, Energies 14 (2021) 1574.

[27] N. Heidari, J. Gwamuri, T. Townsend, J.M. Pearce, IEEE J. Photovoltaics 5 (2015) 1680–1685.

[28] R.E. Pawluk, Y. Chen, Y. She, Renewable and Sustainable Energy Reviews 107 (2019) 171–182.

[29] G. Wirth, M. Schroedter-Homscheidt, M. Zehner, G. Becker, Solar Energy 84 (2010) 215–226.

[30] S. Pelland, G. Galanis, G. Kallos, Progress in Photovoltaics: Research and Applications 21 (2013) 284–296.

[31] E. Lorenz, D. Heinemann, C. Kurz, Progress in Photovoltaics: Research and Applications 20 (2012) 760–769.

[32] A.N.N. Afifah, Indrabayu, A. Suyuti, Syafaruddin, (2021).

[33] X. Li, Q. Yang, Z. Chen, X. Luo, W. Yan, IET Renewable Power Generation 11 (2017) 1234–1244.

[34] J.L. Braid, D. Riley, J.M. Pearce, L. Burnham, in: 2020 47th IEEE Photovoltaic Specialists Conference (PVSC), IEEE, Calgary, AB, Canada, 2020, pp. 1510–1516.

[35] A. Petsiuk, J.M. Pearce, Journal of Manufacturing Science and Engineering 143 (2021).

[36] S.S. Sule, A.L. Petsiuk, J.M. Pearce, Instruments 3 (2019) 30.

[37] Ecodirect, EcoDirect (2022).

[38] Solectria, Yaskawa Solectria Solar (2022).

[39] Canadian Solar, Canadian Solar (2022).

[40] Solectria, Yaskawa Solectria Solar (2022).

[41] Google, Google Colab (2022).

[42] Apogee Instruments, Apogee Instruments, Inc. (2022).

[43] NOAA, National Centers for Environmental Information (2022).

[44] D. Wang, S. Liang, T. He, Y. Yu, C. Schaaf, Z. Wang, Journal of Geophysical Research: Atmospheres 120 (2015) 4825–4841.

[45] Solcast, (2021).

[46] J.M. Freeman, N.A. DiOrio, N.J. Blair, T.W. Neises, M.J. Wagner, P. Gilman, S. Janzou, System Advisor Model (SAM) General Description (Version 2017.9.5), 2018.

[47] J.M. Pearce, P. Mayville, A. Petsiuk, K.S. Hayibo, L. Brown, Open Science Framework (2021).

[48] OpenCV, Open Source Computer Vision (2021).

[49] Weatherspark, February 2021 Weather History in Escanaba Michigan, United States (2022).

[50] L. Powers, J. Newmiller, T. Townsend, in: 2010 35th IEEE Photovoltaic Specialists Conference, IEEE, Honolulu, HI, USA, 2010, pp. 000973–000978.

[51] E. Molin, B. Stridh, A. Molin, E. Wäckelgård, IEEE Journal of Photovoltaics 8 (2018) 1457–1463.

[52] C.D. Rodríguez-Gallegos, M. Bieri, O. Gandhi, J.P. Singh, T. Reindl, S.K. Panda, Solar Energy 176 (2018) 412–438.

[53] J. Bogenrieder, C. Camus, M. Hüttner, P. Offermann, J. Hauch, C.J. Brabec, Journal of Renewable and Sustainable Energy 10 (2018) 021005.

[54] D. Riley, L. Burnham, B. Walker, J.M. Pearce, in: 2019 IEEE 46th Photovoltaic Specialists Conference (PVSC), 2019, pp. 0558–0561.

[55] R.A. Williams, D.J. Lizzadro-McPherson, J.M. Pearce, (2022).

[56] F. Wang, T. Xie, J. Ou, M. Xue, W. Li, Journal of Alloys and Compounds 823 (2020) 153702.

[57] R.W. Andrews, A. Pollard, J.M. Pearce, in: 2013 IEEE 39th Photovoltaic Specialists Conference (PVSC), IEEE, Tampa, FL, USA, 2013, pp. 0229–0234.

[58] R.W. Andrews, A. Pollard, J.M. Pearce, IEEE J. Photovoltaics 5 (2015) 1626–1635.

[59] X. Wang, X. Gao, X. Zhang, W. Wang, F. Yang, Remote Sensing 12 (2020) 485.

[60] M. Macenko, M. Niethammer, J.S. Marron, D. Borland, J.T. Woosley, Xiaojun Guan, C. Schmitt, N.E. Thomas, in: 2009 IEEE International Symposium on Biomedical Imaging: From Nano to Macro, IEEE, Boston, MA, USA, 2009, pp. 1107–1110.